The nature of high-energy radiation damage in iron

2013 J. Phys.: Condens. Matter 25 125402

(http://iopscience.iop.org/0953-8984/25/12/125402)

J. Phys.: Condens. Matter **25** (2013) 125402 (7pp) doi:10.1088/0953-8984/25/12/125402

The nature of high-energy radiation damage in iron

E Zarkadoula[1,5], S L Daraszewicz[2], D M Duffy[2], M A Seaton[3], I T Todorov[3], K Nordlund[4], M T Dove[1] and K Trachenko[1,5]

[1] Queen Mary University of London, Mile End Road, London E1 4NS, UK
[2] London Centre for Nanotechnology, Department of Physics and Astronomy, University College London, Gower Street, London WC1E 6BT, UK
[3] Computational Science and Engineering Department, CCLRC Daresbury Laboratory, Keckwick Lane, Daresbury, Warrington, Cheshire WA4 4AD, UK
[4] University of Helsinki, PO Box 43, FI-00014 Helsinki, Finland

E-mail: e.zarkadoula@qmul.ac.uk

Received 18 November 2012, in final form 7 January 2013
Published 28 February 2013
Online at stacks.iop.org/JPhysCM/25/125402

Abstract
Understanding and predicting a material's performance in response to high-energy radiation damage, as well as designing future materials to be used in intense radiation environments, requires knowledge of the structure, morphology and amount of radiation-induced structural changes. We report the results of molecular dynamics simulations of high-energy radiation damage in iron in the range 0.2–0.5 MeV. We analyze and quantify the nature of collision cascades both at the global and the local scale. We observe three distinct types of damage production and relaxation, including reversible deformation around the cascade due to elastic expansion, irreversible structural damage due to ballistic displacements and smaller reversible deformation due to the shock wave. We find that the structure of high-energy collision cascades becomes increasingly continuous as opposed to showing sub-cascade branching as reported previously. At the local length scale, we find large defect clusters and novel small vacancy and interstitial clusters. These features form the basis for physical models aimed at understanding the effects of high-energy radiation damage in structural materials.

(Some figures may appear in colour only in the online journal)

1. Introduction

Radiation effects are common in Nature. Their sources vary from cosmic radiation to decay of isotopes in terrestrial rocks. A large variety of radiation sources are also created and used in science and technology. This includes energy generation in existing nuclear power stations, where kinetic energy of fission products is converted into heat and electricity. When feasible, future fusion reactors will harvest the energy from thermonuclear reactions. In these applications, the energy of emitted particles has a twofold effect: on one hand, this energy is converted into useful energy, by heating the material; on the other hand, this energy damages the material and degrades the properties important for the operation, including mechanical, thermal, transport and other properties. This is currently a central issue for fusion reactors, where the ability of metal structural components to withstand very high neutron fluxes and other types of radiation such as that of He is intensively discussed [1–3]. Another example is the damage to nuclear reactor materials coming from fission products. In addition, the nuclear industry faces yet another problem, that of radiation damage to materials to be used to encapsulate long-lived radioactive waste [4, 6, 7].

A heavy energetic particle displaces atoms on its path which, in turn, displace other atoms in the system. A collection of these atoms is often referred to as a 'collision cascade' [8–14]. A typical collision cascade created by a heavy 100 keV particle propagates and relaxes in a time on the order of picoseconds and spans nanometers. The resulting structural damage—in the form of amorphous

[5] SEPnet.

pockets or point defects and their clusters—and its long-term evolution ultimately define to what extent the materials' mechanical, thermal and other properties are altered. For example, radiation-induced defects can reduce materials' thermal conductivity and therefore result in inefficient energy transfer in both fusion and nuclear reactors, heat localization and other unwanted effects.

Understanding and predicting these and other effects, as well as designing future materials to be used in intense radiation environments, requires developing physical models. These, in turn, are based on the knowledge of what high-energy radiation damage is in terms of structure and morphology.

Molecular dynamics (MD) simulations have been an important method for studying radiation damage in materials because they give access to the small time and length scales of the collision cascades, and give a detailed picture of the damage at the atomistic scale. Previous MD simulations have provided important insights into the radiation damage process [8–16]. However, due to system size limitations in MD simulations, the reported results were limited to energies of about 100 keV.

On the other hand, knock-on energies are larger in several important applications. When impacted on 14 MeV neutrons, iron knock-on atoms in fusion reactors reach energies of up to 1 MeV [2, 9, 17] with an average energy of about 0.5 MeV [15]. In fission nuclear reactions, the fission product energies are on the order of 50–100 MeV, transferring high energy to the surrounding material. The need to simulate realistic energy cascades has been particularly emphasized, with a view that extrapolation of low-energy results may not account for some important features of higher-energy radiation process which can contain novel qualitative features. More generally, the need to simulate length and energy scales that are relevant and appropriate to a particular physical process has been recognized and reiterated [5].

In this paper, we study the radiation damage process due to high-energy Fe knock-on atoms of 0.2–0.5 MeV energy. We focus on high-energy radiation damage in α-iron, the main structural material in fusion and future fission reactors. We analyze and quantify the nature of collision cascades both at the global and the local scale. We find that high-energy collision cascades may propagate and relax as increasingly continuous damage structures as opposed to showing sub-cascade branching as assumed previously. At the local length scale, we find large clusters and new defect structures.

2. Methods

We have used the DL_POLY program, a general-purpose package designed for large-scale simulations [18, 19]. We have simulated systems with 100–500 million atoms, and run MD simulations on 20 000–60 000 parallel processors of the HECToR National Supercomputing Service [20]. MD simulations were performed for a constant energy and volume ensemble (except for the boundary layer atoms; see below) with an initial temperature set to 300 K, which was preceded by equilibration runs in a constant pressure ensemble at 300 K. Periodic boundary conditions were imposed in all directions.

We have implemented several features to handle radiation damage simulations. First, we used a variable time step to account for faster atomic motion at the beginning of the cascade development and its gradual slowing down at later stages. Second, the MD box boundary layer of thickness of about 10 Å was connected to a constant temperature thermostat at 300 K to emulate the effect of energy dissipation into the sample. Third, we have accounted for the electronic energy losses (EEL), particularly important at high energies. EEL is a complicated process that involves a wide range of effects affecting damage production and annealing [2, 21–23]. Taking EEL into account in MD simulations involves models that include the slowing down of atoms due to energy transfer to electron excitation processes as well as feeding this energy back to the system as the phonon energy. The implementation of this dual energy exchange mechanism in MD simulations, based on the two-temperature approach [22, 24, 55], is in progress. In this work, we model electronic energy loss as a friction term added to the equations of motion. The characteristic energy loss relaxation time (taken here as $\tau_{es} = 1.0$ ps) is obtained by relating the stopping strength ($\lambda = 0.1093$ eV$^{1/2}$ Å^{-1}) [28] in the low-velocity regime via Lindhard's model to the rate of energy loss for a single atom [24, 56]. Such electronic stopping would only be effective above a certain threshold, where the atoms would have sufficient energy to scatter inelastically. We use a cutoff kinetic energy value (8.6 eV) corresponding to twice the cohesive energy [57]; however a number of other threshold values have been proposed [58–61].

For α-Fe, we have used a many-body embedded-atom potential [25], optimized for better reproduction of several important properties of α-Fe including the energetics of point defects and their clusters ('M07' from [26]). At distances shorter than 1 Å, interatomic potentials were joined to short-range repulsive ZBL potentials [28]. The joining was calibrated against the threshold displacement energies [26]. The resulting thresholds were found to be in as good agreement with experiments as the best previous potentials [26, 27].

To analyze the collision cascade, we have employed two methods. First, an atom is identified as 'displaced' if it moves more than distance d from its initial position. The number of displaced atoms, N_{disp}, quantifies the overall amount of introduced damage. Some of this damage recovers back to crystal. To account for this effect, we employed the second method in which an atom is identified as a 'defect'. An atom is considered an 'interstitial' if it is closer to any of the crystalline positions (provided by the initial crystalline reference frame) than distance d and if there is already an atom that is closer to that crystalline site than d. A 'vacancy' is defined as a crystalline position (again provided by the initial crystalline reference frame) for which no atom exists that is closer to it than d. We calculate the number of defect atoms N_{def} as the sum of interstitials and vacancies. Then, N_{def} quantifies both damage production and its recovery. We note that N_{disp} and N_{def} depend on d (we use $d = 0.75$ Å

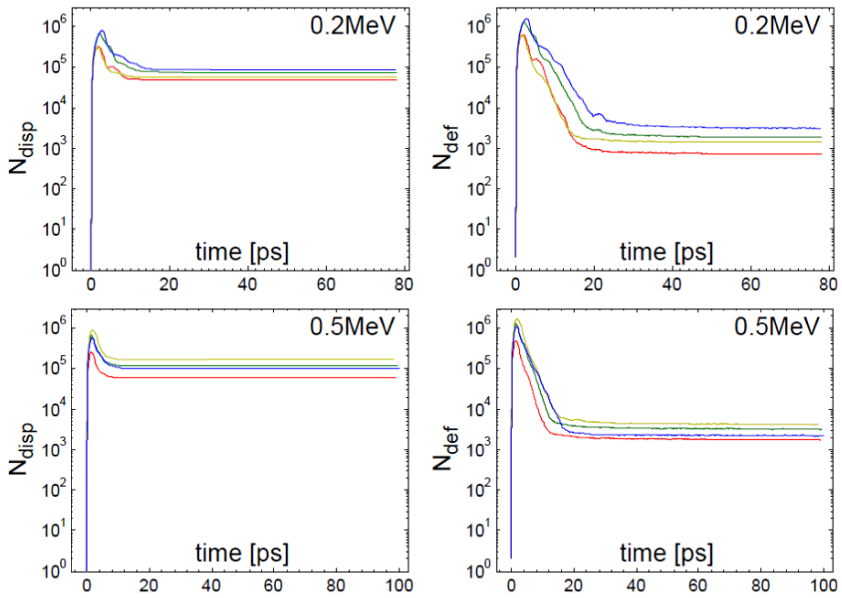

Figure 1. $N_{\rm disp}$ and $N_{\rm def}$ from 0.2 MeV (top) and 0.5 MeV (bottom) knock-on atoms for four cascades.

as a convenient measure). However, the trends discussed in section 3, including the two regimes of cascade relaxation as well as the dynamics of defect recovery, are not sensitive to d provided it is in the sensible range of distances (e.g., too small d, $\lesssim 0.1 - -0.2$ Å, will be affected by usual thermal fluctuations whereas $d \gtrsim 1$–1.5 Å may not identify defect atoms).

Vacancies or self-interstitial atoms (SIA) are defined as belonging to the same defect group (cluster) if they are within two nearest-neighbor distances (plus a 20% perturbation). Second-nearest-neighbor (2nn) distance is a common clustering criterion for SIAs [17, 40]; however the criteria for vacancy clusters vary significantly (from 1nn to 4nn positioning) across the literature [51]. When identifying cluster size in the section 3 the net defect number (the difference between the number of SIAs and the number of vacancies) is reported.

3. Results and discussion

3.1. Large-scale damage

We discuss the main features of high-energy collision cascades. To account for potentially different collision cascades due to different knock-on directions, we have simulated four different directions for each energy, avoiding low-density directions and associated channeling.

$N_{\rm disp}$ and $N_{\rm def}$ are shown in figure 1 for 0.2 and 0.5 MeV cascades simulated in different knock-on directions. We observe three distinct types of damage relaxation.

The first type is related to the large peak of $N_{\rm disp} \approx 10^6$ at short times of about 1–2 ps. This peak relaxes during about 10 ps. This peak is often discussed as the 'thermal spike' [30–32], a phenomenological picture that explores the similarity between the atomic motions in the collision cascade and local melting. In this picture, a collision cascade has reduced density because melts have smaller density compared to their solid phases. We note here that the density of some melts (e.g. of Si, of H_2O and others) around the melting point is actually larger than the density of their parent solid compounds, and hence this explanation cannot be generally used. In addition, the atomic motions and local density fluctuations in the melt and in the collision cascade are qualitatively different.

We propose that at the atomistic level, the increase of $N_{\rm disp}$ can be understood on the basis of anharmonicity of interatomic interactions: large-scale atomic motion inside the cascade causes increase of the interatomic separations due to anharmonicity. This results in the outward pressure from the cascade on the surrounding lattice and lattice expansion. This elastic deformation lasts several ps, equal to several periods of atomic vibrations during which the energy is dissipated to the lattice, and gives rise to the peak of $N_{\rm disp}$. Notably, the elastic deformation is reversible irrespective of whether or not it is followed by the recovery of the structural damage discussed below. In figure 1, $N_{\rm disp}$, averaged over all knock-on directions at the end of the simulation (corresponding to the flat lines in figure 1), is about 67 000 and 111 000 atoms for 0.2 MeV and 0.5 MeV cascades, respectively.

Figures 2 and 3 show the snapshots of the collision cascades at three different stages of cascade development that include the intermediate stage corresponding to the large peak of $N_{\rm disp}$ in figure 1. We observe, consistent with figure 1, a significantly larger number of atoms involved in large displacements at intermediate times as compared to the final relaxed state.

The second type of cascade relaxation is related to the dynamics of $N_{\rm def}$. At short ps times, the large peak of $N_{\rm def}$ is of the same origin as that seen for $N_{\rm disp}$. However, the dynamics of $N_{\rm def}$ also reflects the recovery of structural damage due to ballistic displacements. This recovery proceeds by the diffusion and recombination processes during which atoms settle at the newly found crystalline positions. This process lasts up to 20 ps, significantly longer than the relaxation time

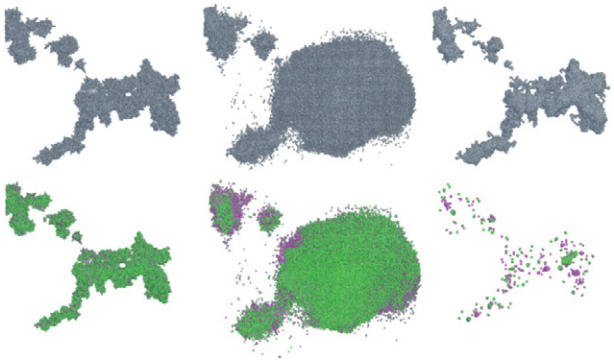

Figure 2. Displaced (top) and defect (bottom) atoms in a representative 0.2 MeV collision cascade. The knock-on atom moves from the top left to the bottom right corner. The three frames for each atom type correspond to 0.3 ps, 3 ps and 80 ps, respectively. The cascade size (maximal separation between any two atoms in the cascade) is 560 Å. Vacancies (interstitials) are represented in purple (green); we used Atomeye software [29] to visualize the cascade evolution.

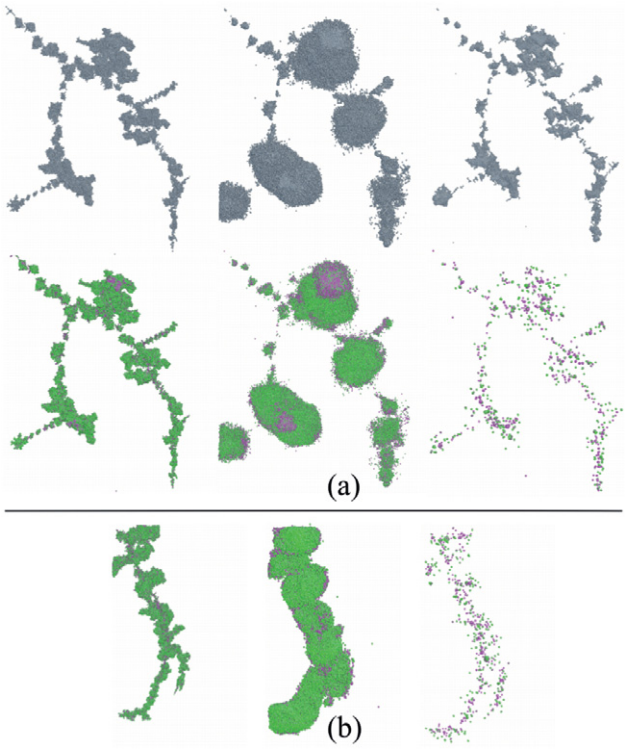

Figure 3. (a), (b) show two representative 0.5 MeV cascades. The knock-on atom moves from the top left to the bottom right corner. In (a) we show both displaced (top) and defect (bottom) atoms at 0.2, 1.5 ps and 100 ps. In (b) we show the defect atoms only at 0.3 ps, 2 ps and 100 ps. The cascade size in (a) and (b) is 950 Å and 1300 Å, respectively.

of the first elastic relaxation process (see figure 1). As a result of this relaxation, N_{def}, averaged over all simulated directions at the end of the simulation (corresponding to the flat lines in figure 1), is about 1800 and 2800 atoms for 0.2 MeV and 0.5 MeV cascades, respectively, corresponding to an approximately 97% recovery rate as compared to N_{disp}. Such a high recovery rate is in interesting resemblance to those of some of the resistant ceramic materials, but in contrast to those of others [33, 34].

We also find that N_{disp} and N_{def} reported in figure 1 include displaced and defect atoms that are located throughout the simulation box and away from the moving recoils. This damage appears in the structure during very short times of 0.1–0.2 ps (before the peak of the damage shown in figure 1) and in locations that fast recoils have not yet reached, and can therefore not be due to direct ballistic hits. Consequently, we attribute this damage to the shock wave induced by fast recoils. Indeed, the initial velocity of the 500 keV primary recoil atom is about 1314 km s^{-1}, or approximately 260 times faster than the speed of sound in iron. Interestingly, we observe displacements induced by the shock wave using the fairly large cutoff displacements distance ($d = 0.75$ Å as discussed above). For 500 keV recoils, N_{disp} and N_{def} due to the shock wave peak are approximately 120 each, i.e. involve much smaller numbers than those involved in two previous types of damage relaxation. After about 0.2 ps, both defect and displaced atoms induced by the shock wave disappear and relax back to crystalline positions. Similarly to elastic deformation around the cascade, the deformation due to the shock wave is reversible, although it operates on a much shorter time scale.

Our simulations provide an important insight into the structure and morphology of high-energy cascades. The existing view of collision cascades is that they branch out to smaller sub-cascades and 'pockets' of damage that are well separated from each other [17]. This takes places over a certain energy threshold, even though this threshold has not been firmly established [17, 35, 36]. We note that in materials resistant to amorphization such as metals and certain oxides, these sub-cascades and pockets of structural damage exist on the short time scale of several ps only, as is seen in figure 1, and subsequently recover to form point defects as discussed below. On the other hand, the sub-cascades recover poorly in amorphizable materials [46], forming highly disordered structures that result in permanent amorphization. In either case, cascade branching (or the absence of branching) governs the distribution of the final damage and its morphology.

This picture originated as a result of using binary-collision simulations in combination with MD simulations of low-energy events. Although involving approximations inherent in binary-collision simulations and extrapolations of low-energy MD simulations, this picture would offer a great degree of reduction and simplification: in analyzing the results and consequences of high-energy damage, only small sub-cascades need to be considered.

In figures 2 and 3, we observe a qualitatively different picture. Cascade branching is visibly reduced as compared to low-energy events, in that we do not find well-separated sub-cascades. Some cascade branching is seen in the first 0.5 MeV cascade shown in figure 3(a) only and, importantly, during an intermediate stage of cascade development only. On the other hand, the final cascade morphology is described by a rather continuous distribution of the damage across about 1000–1300 Å where no distinctly separated sub-cascades can be identified. Common to all collision cascades that we have

Table 1. The number of Frenkel pairs (FPs; N_F), and defect statistics for 0.2 and 0.5 MeV cascade simulations in α-iron. The value in brackets shows the standard error in the mean over four constituent runs for each simulation. The largest clusters are determined by the net defect count. The NRT fraction is the normalized number of FPs [50].

Cascade energy	N_F	NRT fraction of defects	Number of isolated vacancies	Number of split SIAs	Number of vacancy clusters	Number of SIA clusters	Largest vacancy cluster	Largest SIA cluster
0.2 MeV	900 (200)	0.44 (0.11)	70 (5)	65 (4)	17 (1)	46 (7)	54	89
0.5 MeV	1450 (220)	0.29 (0.04)	150 (14)	170 (15)	36 (7)	84 (13)	47	36

simulated, this picture is particularly visible for defect atoms in the final state of the cascades shown in figures 2 and 3.

Qualitatively, reduced cascade branching and the emergence of a more continuous damage distribution can be understood as follows. For a scattered atom to move far enough from its initial position and form a spatially separated sub-cascade (i.e., branch out) requires a large amount of energy transferred to it by the incident atom. In the absence of inelastic losses, the transferred energy, T, is $T = \frac{1}{2}T_m(1 - \cos(\phi))$, where T_m is the maximal transferred energy and ϕ is the scattering angle [37]. For large energy of the incident atom, E, ϕ decreases as $\phi \propto \frac{1}{E}$ [37]. We therefore find that for large E and small ϕ, T decreases as $T \propto \phi^2 \propto \frac{1}{E^2}$. Large E and, consequently, small T, results in scattered atoms forming the damaged region close to the trajectory of the initial knock-on atom and, therefore, promote a continuous structure of the resulting damage. This is consistent with our current findings.

Interestingly, an increasingly continuous structure of cascade morphology observed here is consistent with that seen in irradiation experiments using swift heavy ions [46]. This suggests that the energies simulated in this work broadly correspond to the crossover between the branched and continuous cascade morphologies.

We note that as the incident atom slows down, T increases, leading to sub-cascade branching at the end of the atom trajectory. However, larger E results in an increase of the relative fraction of continuous damage over the fraction of branched cascades.

Our finding is important in the context of the long-term evolution of radiation damage. Indeed, a recent kinetic Monte Carlo study [40] has shown that very large defect clusters can have a major effect on the long-term damage development.

3.2. Local defects and their clusters

The discussion has so far concentrated on the large-scale cascade structure and morphology. We now briefly discuss defect structures at the local level.

Several mechanisms for local defect clustering have been discussed in the literature. Vacancies have been shown to cluster by the recrystallization front around a heat spike, pushing them towards the center of the cascade [38, 39]. This mechanism has been shown to be able to (rarely) produce very large clusters [40]. For the interstitials the situation is more complex. The concept of 'interstitial loop punching', well known to be active around high-pressure gas bubbles [41], was suggested to produce interstitial clusters also around heat spikes [42]. Later research, however, showed that it can produce stable damage only near surfaces [43, 44]. Other works have shown that interstitial clusters can be produced, in the bulk at least, by the isolation of atoms in a liquid pocket left behind a recrystallization front [45] and by shock waves associated with hypersonic recoils [16].

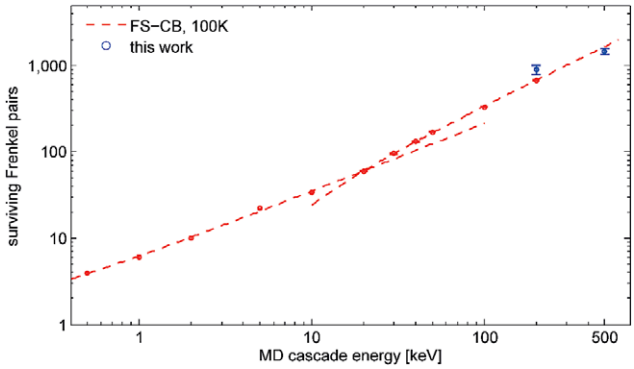

Figure 4. Dependence of the number of surviving FPs on the cascade energy; a comparison between Finnis–Sinclair potential runs started at 100 K (red line [17]) and the current findings (blue). The fits correspond to a single-cascade and sub-cascade (branching) regimes (details appear in [17]). While there are differences in the simulation setups, the number of Frenkel pairs produced at 200 and 500 keV follows the general trend observed for lower-energy cascades.

The size and structure of the defect clusters created by the cascades in this work were analyzed and the results are summarized in table 1. The simulations confirm that the normalized fraction of Frenkel pairs (FPs) of 0.3–0.4 is roughly constant for cascades over 0.1 MeV [17, 51]. The number of surviving FPs follows the trend from lower cascade energies (figure 4). The fraction of surviving interstitials grouped into clusters was found to be 0.58(3) and 0.52(3) for cascade energies of 0.2 and 0.5 MeV, respectively. This is consistent with the results for 50–100 keV cascades [17, 40] hinting at a possibility that the clustering fraction may reach a maximum at ~100 keV. A similar trend was observed for vacancy clustering fractions of 0.33(3) and 0.35(1), respectively.

The majority of interstitial clusters were found to be glissile $\langle 111 \rangle$ crowdion clusters, and some of those form dislocation loops with a Burgers vector of $b = (1/2)\langle 111 \rangle$. This is in line with the recent theoretical [47] and

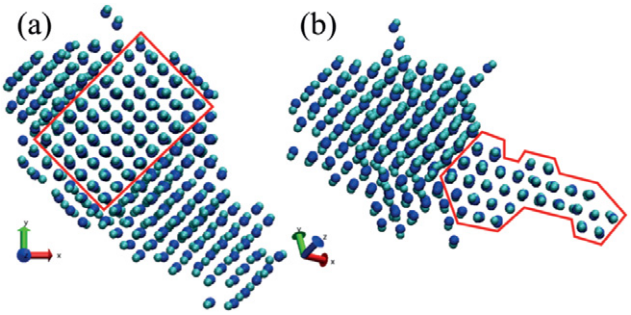

Figure 5. The largest cluster consisting of 89 interstitials. It is mainly composed of a set of ⟨100⟩ crowdions (the selected region in (a)) and a fraction of normally glissile ⟨111⟩ crowdions (the region highlighted in (b)). Such cluster morphology blocks the motion of crowdions and results in an overall sessile cluster; a similar effect of immobilization of a cluster by another defect was observed in [52]. Interstitials (vacancies) are shown in silver (blue). We used the VMD package for visualization of local defect structures [53].

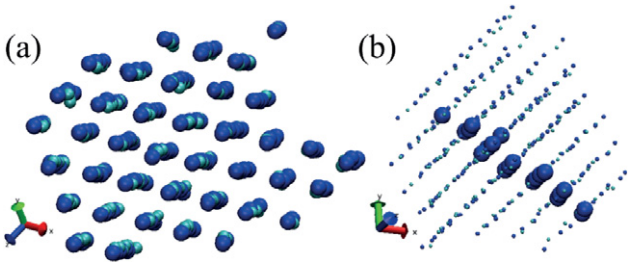

Figure 6. (a) A (111) projection of a 39-vacancy cluster; (b) a (001) projection of this cluster. The large spheres show the central vacancy for selected constituent 'vacancy crowdions', thus emphasizing the dislocation nature of the cluster.

experimental results [48], which indicate that for temperatures smaller than 600 K, the $b = (1/2)\langle 111\rangle$-type loops are stable, whereas $b = \langle 001\rangle$ ones are unstable. The largest defect structure was a composite 89-interstitial cluster, formed from a merging of a set of ⟨111⟩ and ⟨100⟩ crowdions (figure 5). Owing to its complex morphology, it will be immobile. This interstitial cluster is quite large, yet consistent with the data reported for lower energies [40, 49].

Large vacancy clusters were also observed, with the 54-vacancy cluster being the largest one. Several large vacancy clusters formed ⟨100⟩ and ⟨111⟩ dislocation loop-like configurations (figure 6(a)). A cross section of an exemplar vacancy cluster is shown (figure 6(b)), to emphasize its dislocation-like nature. The smaller vacancy clusters revealed a rich variety of structures, such as hexagonal vacancy clusters with interstitial rings surrounding a central vacancy (figure 7(a)).

We also observed a wide range of sessile interstitial clusters. Some of these could be clearly identified as being related to the C15 metastable phase discussed in [54], and many were joined to crowdions or crowdion clusters (figure 7(b)). Smaller ring-like structures were also observed (figure 7(c)) in which six atoms shared four neighboring lattice sites.

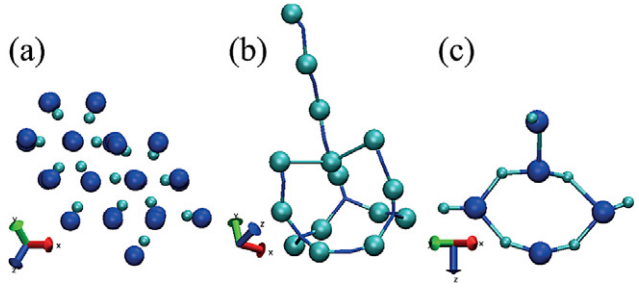

Figure 7. (a) The (111) projection of a small nine-vacancy cluster; (b) a C15 phase tetra-interstitial with a ⟨111⟩ crowdion attached; the vacancies are omitted from the figure for clarity; (c) a hexagonal di-interstitial with a split interstitial attached.

4. Conclusions

In summary, we have found novel structural features of radiation damage in iron on both large and local scales which will need to be included in physical models aimed at understanding and predicting the effects of radiation damage on the mechanical, thermal and transport properties of structural materials. The reported damage structures such as the increased continuous morphology of high-energy collision cascades will form a starting point for long-time-scale models, developed in order to understand and predict the effects of radiation damage. The large defect structures reported here, including novel vacancy and interstitial clusters, will be important for the understanding of the interaction of these clusters with transmutation gases and the nucleation of helium bubbles.

Acknowledgments

Via our membership of the UK's HPC Materials Chemistry Consortium, which is funded by EPSRC (EP/F067496), this work made use of the facilities of HECToR, the UK's national high-performance computing service, which is provided by UoE HPCx Ltd at the University of Edinburgh, Cray Inc. and NAG Ltd, and funded by the Office of Science and Technology through EPSRC's High End Computing Programme.

References

[1] Ward D J and Dudarev S L 2008 *Mater. Today* **11** 46
[2] Stoneham A M, Matthews J R and Ford I J 2004 *J. Phys.: Condens. Matter* **16** S2597
[3] Dudarev S L *et al* 2009 *J. Nucl. Mater.* **386** 1
[4] Weber W J *et al* 1998 *J. Mater. Res.* **13** 1434
[5] Stoneham A M and Harding J H 2003 *Nature Mater.* **2** 77
[6] Ringwood A E *et al* 1981 *Nucl. Chem. Waste Manag.* **2** 287
[7] Geisler T, Trachenko K, Rios S, Dove M T and Salje E K H 2003 *J. Phys.: Condens. Matter* **15** L597
[8] Averback R S and Diaz de la Rubia T 1998 *Solid State Physics* vol 51, ed H Erhenfest and F Spaepen (New York: Academic) p 281
[9] Ishino S, Schiller P and Rowcliffe A F 1989 *J. Fusion Energy* **8** 147
[10] Nordlund K 2002 *Nucl. Instrum. Methods Phys. Res.* B **188** 41

[11] Souidi A *et al* 2006 *J. Nucl. Mater.* **355** 89
[12] Calder A F, Bacon D J, Barashev A V and Osetsky Y N 2008 *J. Nucl. Mater.* **382** 91
[13] Morishita K and Diaz de la Rubia T 1999 *J. Nucl. Mater.* **271** 35
[14] Bacon D J *et al* 2003 *J. Nucl. Mater.* **323** 152
[15] Stoller R E and Greenwood L R 1999 *J. Nucl. Mater.* **271/272** 57
[16] Calder A F, Bacon D J, Barashev A V and Osetsky Yu N 2010 *Phil. Mag.* **90** 863
[17] Stoller R E 2012 *Comprehensive Nuclear Materials* vol 1, ed R J M Konings (Amsterdam: Elsevier) p 293
[18] Todorov I T, Smith B, Trachenko K and Dove M T 2005 *Capability Comput.* **6** 12
[19] Todorov I T, Smith B, Dove M T and Trachenko K 2006 *J. Mater. Chem.* **16** 1911
[20] www.hector.ac.uk
[21] Race C P *et al* 2010 *Rep. Prog. Phys.* **73** 116501
[22] Rutherford A M and Duffy D M 2007 *J. Phys.: Condens. Matter* **19** 496201
[23] Caro A and Victoria M 1989 *Phys. Rev.* A **40** 2287
[24] Duffy D M and Rutherford A M 2009 *J. Nucl. Mater.* **386–388** 19
[25] Mendelev M I *et al* 2003 *Phil. Mag.* **83** 3977
[26] Malerba L *et al* 2010 *J. Nucl. Mater.* **406** 19
[27] Nordlund K, Wallenius J and Malerba L 2005 *Nucl. Instrum. Methods Phys. Res.* B **246** 322
[28] Ziegler J F, Biersack J P and Littmark U 1985 *The Stopping and Range of Ions in Matter* (New York: Pergamon)
[29] Li J 2003 *Modelling Simul. Mater. Sci. Eng.* **11** 173
[30] Brinkman J A 1954 *J. Appl. Phys.* **25** 961
[31] Diaz de la Rubia T, Averback R S, Benedeck R and King W E 1987 *Phys. Rev. Lett.* **59** 1930
[32] Samela J and Nordlund K 2008 *Phys. Rev. Lett.* **101** 027601
[33] Trachenko K, Dove M T, Artacho E, Todorov I T and Smith W 2006 *Phys. Rev.* B **73** 174207
[34] Trachenko K, Pruneda M, Artacho E and Dove M T 2005 *Phys. Rev.* B **71** 184104
[35] Nordlund K, Wei L, Zhong Y and Averback R S 1998 *Phys. Rev.* B **57** 13965
[36] Heinisch H L, Singh B N and Diaz de la Rubia T 1994 *J. Nucl. Mater.* **212–215** 127
[37] Smith R 1997 *Atomic and Ion Collisions in Solids and at Surfaces* (Cambridge: Cambridge University Press)
[38] Nordlund K and Averback R S 1999 *Phys. Rev.* B **59** 20
[39] Nordlund K and Averback R S 2000 *J. Nucl. Mater.* **276** 194
[40] Björkas C, Nordlund K and Caturla M J 2012 *Phys. Rev.* B **85** 024105
[41] Trinkaus H and Wolfer W G 1984 *J. Nucl. Mater.* **122/123** 552
[42] Diaz de la Rubia T and Guinan M W 1991 *Phys. Rev. Lett.* **66** 2766
[43] Diaz de la Rubia T 1996 *Nucl. Instrum. Methods Phys. Res.* B **120** 19
[44] Nordlund K, Keinonen J, Ghaly M and Averback R S 1999 *Nature* **398** 49
[45] Nordlund K *et al* 1998 *Phys. Rev.* B **57** 7556
[46] Trachenko K 2004 *J. Phys.: Condens. Matter* **16** R1491
[47] Dudarev S *et al* 2008 *Phys. Rev. Lett.* **100** 135503
[48] Yao Z *et al* 2010 *Phil. Mag.* **90** 4623
[49] Soneda N, Ishino S and Diaz de la Rubia T 2001 *Phil. Mag. Lett.* **81** 649
[50] Norgett M J, Robinson M T and Torrens I M 1975 *Nucl. Eng. Des.* **33** 50
[51] Malerba L 2006 *J. Nucl. Mater.* **351** 28
[52] Gao F, Bacon D J, Osetsky Y N, Flewitt P E J and Lewis T A 2000 *J. Nucl. Mater.* **276** 213
[53] Humphrey W, Dalke A and Schulten K 1996 *J. Mol. Graph.* **14** 33
[54] Marinica M-C, Willaime F and Crocombette J-P 2012 *Phys. Rev. Lett.* **108** 025501
[55] Anisimov S I, Kapeliovich B L and Perel'man T L 1974 *Zh. Eksp. Teor. Fiz.* **66** 776
Anisimov S I, Kapeliovich B L and Perel'man T L 1974 *Sov. Phys.—JETP* **39** 375 (Engl. transl.)
[56] Lindhard J and Scharff M 1961 *Phys. Rev.* **124** 128
[57] Zhurkin E and Kolesnikov A 2003 *Nucl. Instrum. Methods Phys. Res.* B **202** 269
[58] Jakas M and Harrison D 1985 *Phys. Rev.* B **32** 2752
[59] Nordlund K, Zhong L and Averback R 1998 *Phys. Rev.* B **57** 965
[60] le Page J, Mason D R, Race C P and Foulkes W M C 2009 *New J. Phys.* **11** 013004
[61] Björkas C and Nordlund K 2009 *Nucl. Instrum. Methods Phys. Res.* B **267** 1830